DAVID G. TILLEY

SIR-B OCEAN-WAVE ENHANCEMENT WITH FAST FOURIER TRANSFORM TECHNIQUES

Shuttle Imaging Radar (SIR-B) imagery is Fourier filtered to remove the estimated system-transfer function, reduce speckle noise, and produce ocean scenes with a gray scale that is proportional to wave height. The SIR-B system response to speckled scenes of uniform surfaces yields an estimate of the stationary wavenumber response of the imaging radar, modeled by the 15 even terms of an eighth-order two-dimensional polynomial. Speckle can also be used to estimate the dynamic wavenumber response of the system due to surface motion during the aperture synthesis period, modeled with a single adaptive parameter describing an exponential correlation along track. A Fourier filter can then be devised to correct for the wavenumber response of the remote sensor and scene correlation, with subsequent subtraction of an estimate of the speckle noise component. A linearized velocity bunching model, combined with a surface tilt and hydrodynamic model, is incorporated in the Fourier filter to derive estimates of wave height from the radar intensities corresponding to individual picture elements.

INTRODUCTION

The concept of a wave spectrum[1] for describing wind-generated surface waves has served oceanographers well over the last quarter century. Using spaceborne radar observations, regular ocean-wave fields induced by distant storms have recently[2] been Fourier analyzed to estimate directional wavenumber spectra for oceanographic applications. However, anomalous wave groups,[3] not necessarily characterized by the normal statistics of the spectral approach, might be better examined directly from appropriately corrected synthetic aperture radar (SAR) images of the sea surface. Furthermore, knowledge of the spatial distribution of wave groups in a crossed or "lumpy" sea (see the article by Mollo-Christensen, this issue) may provide insight into the importance of wave–wave interactions that could not be inferred from an estimate of the directional spectrum only. Thus, it seems appropriate to apply what has been learned about the SAR ocean-imaging modulation transfer function in the spectral domain to derive estimates of surface height in the image domain.

Spatial signatures of individual wave groups are preserved in the complex Fourier transform of the SIR-B image intensity. These characteristic properties reside in the Fourier phase spectrum, which is usually neglected, since it is the Fourier power spectrum that is traditionally associated with the ocean-wave spectrum. The Fourier power and phase are orthogonal quantities in the complex spectral domain, so it is possible to preserve the phase information while performing ordinary arithmetic operations (e.g., multiplication and subtraction) on the power spectrum to implement an ocean-wave modulation-transfer function. Subsequent Fourier inversion of the ocean-wave spectrum, with SIR-B image phase relations intact, will recreate the locations of the original wave groups and will also allow estimates of their height, assuming that the SAR modulation-transfer function is well behaved (i.e., remains linear even for the anomalous wave groups). The resulting height map can be normalized with temporally or spatially averaged independent observations of significant wave height.

Although the modulation-transfer function for azimuth-traveling waves, including all the effects of sea-surface motion, has yet to be completely validated,[4] a tilt modulation model augmented with a linearized velocity-bunching theory[5,6] can be applied to SIR-B image data to convert backscattered intensities for individual picture elements (pixels) to estimates of wave height. One may compute the mean and standard deviation of the restored wave-height data and then use these quantities to plot a surface-elevation distribution function, in the manner of Huang and Long.[7] The results of this exercise, shown in Fig. 1, indicate nearly normal ocean-height distributions for three corrected data sets from SIR-B. Each of the height distributions, derived after having applied the series of steps described below, has been normalized with independent estimates of the significant wave height.

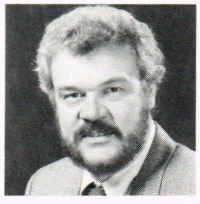

David G. Tilley is a senior staff engineer in the Space Geophysics Group, The Johns Hopkins University Applied Physics Laboratory, Laurel, MD 20707.

THE SIR-B WAVENUMBER RESPONSE FUNCTIONS

Image speckle, resulting from the random coherence of a finite number of specular "events" (i.e., surface facets tilted toward the radar at random locations) oc-

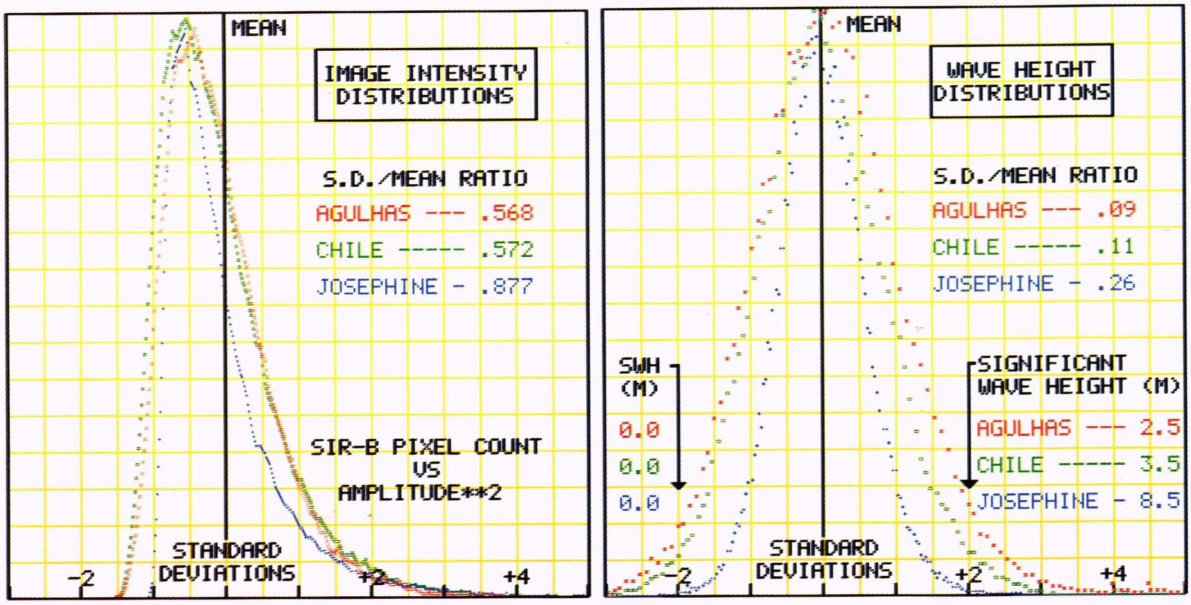

Figure 1—SIR-B image-intensity distributions (left) and restored wave-height distributions (right) for the three Fourier-filtered scenes shown in Fig. 5. The standard-deviation-to-mean ratio is reduced by removing broadband noise from the ocean imagery.

curring within a single resolution cell, adds noise that interferes with scene interpretation. However, this type of broadband noise produces a "white" spectral response that can be useful in estimating the wavenumber response function of the imaging system. In general, the wavenumber response function is the Fourier transform of the point spread function and represents a loss of spatial resolution due to the finite limitations of the remote sensor. For this reason, the wavenumber response function is sometimes called the instrument transfer function.

The SIR-B wavenumber response function, as estimated with orthogonal (range and azimuth) fourth-order polynomials, has been previously reported,[8] based on coherently speckled random data collected by SIR-B over Baie Missisquoi near Montreal, Canada, on October 7, 1984. The separation of the range and azimuth polynomial functions was based on earlier work[9] with a scene of the Chesapeake Bay recorded by the Seasat SAR and was implemented to compare the response characteristics of the Seasat and SIR-B instruments. Although the SIR-B instrument-transfer function estimated with this technique appeared adequate for wavenumbers less than 0.128 ($2\pi/50$) radian per meter, the normalization of the dual polynomial product could not be optimized for both the range and azimuth coordinates simultaneously; this seemed to be a consequence of the unequal SIR-B range and azimuth resolutions. Over Baie Missisquoi, the SIR-B look angle was 34 degrees, compared to a fixed 23 degrees for the Seasat. In addition, the SIR-B range bandwidth was only 12 megahertz compared to the Seasat bandwidth of 20 megahertz. An eighth-order two-dimensional polynomial is now used to characterize the SIR-B instrument-transfer function. The eighth-order polynomial coefficients are optimized by linear regression of the squared fractional error. The higher order model extends the estimation procedure well

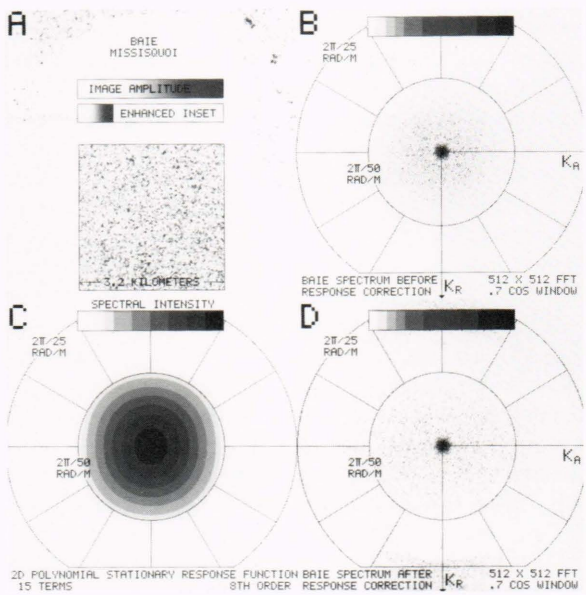

Figure 2—A section of Baie Missisquoi (A) was chosen from SIR-B Data Take A0-037.20, scene 001, as a randomly speckled scene that could be used as an ergodic input to the imaging process. Also displayed is the Fourier power spectrum (B) computed for that scene. Several contours of the two-dimensional polynomial (C) approximating the SIR-B wavenumber response function are shown along with the response-corrected spectrum (D) for Baie Missisquoi.

beyond the $2\pi/50$ radian per meter wavenumber (Fig. 2) and also accommodates the variable look angle of the SIR-B platform.

Since there is a 180-degree ambiguity in a single Fourier wave spectrum, any polynomial function, $P(k,l;i,j)$, used to model the wavenumber response must be an even function of both the range and azimuth wavenumbers,

k and l, respectively. To eighth order, there are 15 such even terms,

$$P(k,l;i,j) = \sum_{i=0,j=0}^{i+j<5} c(i,j) \times k^{2i} \times l^{2j} , \quad (1)$$

including the constant term that dominates at $k=l=0$. The linear regression that computes the best polynomial fit to spectral data, $D(k,l)$, minimizes the squared fractional error,

$$E(i,j) = \sum_{k} \sum_{l} [1-P(k,l;i,j)/D(k,l)]^2 \quad (2)$$

by solving 15 simultaneous equations, $\partial E(i,j)/\partial c(i,j) = 0$, in terms of the 15 polynomial coefficients, $c(i,j)$. The summation over the spectral domain expressed in Eq. 2 is computed several times to include more or less of the data in the linear regression. Hence, the squared fractional error sum for the Baie Missisquoi data is minimized for bounding wavenumber values of k between ± 0.192 and of l between ± 0.240 radians per meter. For the SIR-B instrument, it should be emphasized that the range transfer function is invariant in *slant range*. When the *slant range* database is resampled to the *ground range* perspective, the sine of the incidence angle is used to create ground pixels of dimension 12.5 meters. The ground-range resolution is therefore proportional to the reciprocal sine of the variable look angle and is generally different from the azimuth resolution, which is fixed by the bandwidth of the scene correlator.

The topology of the ocean surface evolves over both short and long time scales due to random and deterministic surface motions. Hence, conventional methods for extracting signals embedded in multiplicative noise are less accurate for ocean scenes than they are for land scenes, since motion occurs during the time required to acquire four independent records of the "unfrozen" surface (i.e., four looks at a changing scene). The ocean surface is also in motion during the single-look integration period of the SIR-B scene correlator, so motion blur is usually evident in the along-track (azimuth) direction. Since the ocean surface is irradiated with short pulses and the reflected radiation is sampled between pulse periods, the along-track synthesis of the Doppler aperture is not continuous in time. Furthermore, the Doppler technique for estimating along-track position inherently assumes no radial surface motion during the interpulse periods. Thus, since a SAR uses a finite interval to measure a nonstationary random variable, one may hypothesize that sample statistics are Poisson distributed, implying that sequential intensity samples are correlated with a characteristic exponential decay $e^{-\lambda y}$, where y is the along-track coordinate, and λ is the spatial decay rate.

The surface velocity distribution is essentially determined by wave motion, but the dynamic wavenumber response is not necessarily uniform over the entire scene. For nonuniform conditions, linear methods for correcting the motion blur will not be entirely accurate. However, if one assumes that the orbital motion of an *ensemble* of waves imparts a radial velocity to the surface, and the velocity is randomly distributed according to the positions of the actual waves constituting the scene, then the dynamic response of the SIR-B to deterministic surface motion may be modeled as a low-pass filter along track. Thus, deterministic surface decorrelation may be treated in the same manner as random decorrelation, here modeled as a one-sided exponential function[10] convolved with the backscatter image of the scene in the along-track direction. Although the model is admittedly somewhat oversimplified, it may be the best linear correction that can be made for SIR-B image data without attempting corrections of complex signal-phase relations prior to square-law detection and multilook averaging. In the Fourier power spectrum of a SIR-B ocean image, motion blur can then be modeled as the product of the ocean-wave spectrum and the Fourier transform of the one-sided exponential distribution function:[11]

$$M(\lambda,l) = \int_{-\infty}^{\infty} \exp(-\lambda|y|)\exp(-ily)dy$$

$$= \lambda/(\lambda^2+l^2) . \quad (3)$$

One can extimate the extent to which a SIR-B scene has been influenced by motion blurring along track by observing the Fourier spectrum of the speckled image. Surface motion has the effect of producing a band of spectral energy at low-azimuth wavenumber (see Fig. 1 in the article by Beal, this issue, for an example of some particularly strong banding in the Seasat data). A data-dependent procedure can be used to correct a SIR-B wave spectrum for the dynamic wavenumber response resulting from surface scatterer motion. To begin the procedure, the Fourier power spectrum is averaged over the range wavenumber to yield a data profile $D(l)$ as a function of azimuth wavenumber only. Then a squared reciprocal error function $R(\lambda)$ is defined as the squared difference between the reciprocal of the data profile and the reciprocal of the azimuth degradation function (e.g., Eq. 3) summed over all azimuth wavenumbers. An estimate of the parameter, λ, is found by setting the derivative $\partial R(\lambda)/\partial\lambda$ equal to zero:

$$\sum_{l} [\lambda^2-l^2-\lambda/D(l)] \times (\lambda^2-l^2)/\lambda^3 = 0 . \quad (4)$$

This equation identifies one data-independent root, $\lambda = <l>$, where $<l>$ is the mean value of l that can be used for the linear numerator term of Eq. 3 in solving

$$\sum_{l} [\lambda^2-l^2-<l>/D(l)] = 0 \quad (5)$$

for its data-dependent root. This procedure essentially scales the solution to the range of wavenumbers under consideration, independent of the data presented. The

dynamic response function estimated in this way can then be applied as a linear correction for the degradation of image resolution along track.

RESTORATION OF OCEAN-WAVE CHARACTERISTICS

A complete definition of a Fourier restoration filter for SIR-B would require a model of the total system modulation transfer function that included all hydrodynamic, electromagnetic, and Doppler motion effects. A better understanding of these effects may eventually emerge from the two-scale scattering model[12] by merging it with the concept of strong but infrequent specular scatterers coherently summed over a single resolution cell. On this short and transient scale, speckle noise arises from random correlations of the irradiating radar bursts with the spatial and temporal locations of specular facets[13] that are at least several Bragg wavelengths and at most several resolution cells in dimension. Image "streakle"[14] results when specular facets have a velocity imparted by the ocean waves that is significant relative to the differential Doppler velocity used for measurement of their along-track position. So speckle is more than a random noise process; it actually contains information that can help characterize the environmentally dependent system transfer function.

The velocity-bunching concept[5] combined with the tilt and hydrodynamic modulation model forms the basis of a standard methodology for converting response-corrected SAR image spectra to ocean-height spectra[15] (see also the articles by Lyzenga and Monaldo, this issue). The ocean-image-to-ocean-height conversions can be accomplished by applying the five-step process discussed by Monaldo in this issue (see his Fig. 1). The removal of the SIR-B stationary wavenumber-response function is neither data dependent nor adaptive but proceeds directly from the Baie Missisquoi analysis previously described. However, the removal of an optional dynamic wavenumber-response function (not shown in Monaldo's figure) is both data dependent and adaptive. As discussed above, the filter can be modeled as the power spectrum of a one-sided exponential distribution that best approximates the actual data envelope in the Fourier domain. Multiplicative speckle noise power is excluded from the data envelope by ignoring spectral components below the 20 percent mean power level.[16] The Fourier spectrum is then smoothed in the wavenumber domain[17] to improve statistical reliability. A spectral noise pedestal is removed by subtracting a constant (defined as the mean spectral density plus one standard deviation) from the Fourier spectrum at all wavenumbers. Smoothing prior to thresholding reduces the likelihood of generating negative power values (negative power values are set to zero when they are encountered), thereby preserving phase relations for a larger wavenumber domain. At this point, the SIR-B power spectrum resembles, but is not identical to, an ocean-wave slope-variance spectrum. The final wave-height spectrum results from dividing the corrected SIR-B instrument spectrum by a two-dimensional hydrodynamic transfer function. This process is held constant at low wavenumbers where both the tilt modulation term and the velocity bunching term fall to zero.

The complex Fourier spectrum may be inverse transformed at any intermediate point in the filtering sequence to observe the effect of all five individual filtering operations, as illustrated in Fig. 3. This low-sea-state image from the Chile data set illustrates particularly well the effectiveness of Fourier filtering algorithms in extracting a weak wind-driven wave system immersed in random clutter, even at wavenumbers approaching the resolution limits of the SIR-B instrument.

The set of filter constraints discussed above is based on an analysis of ocean swell observed in the Chile data set. In general, the constraints are also valid for wind-driven waves, although the fifth stage of the filter might be improved with more appropriate modulation models. Salient properties of the filter, including the empirical estimation of a broadband noise pedestal, are revealed by this severe test of our spectral processing methods when applied to yield the sequential Fourier power spectra in Fig. 4 corresponding to the five-stage Chile imagery.

Four of the five restoration operators that are applied to the complex Fourier spectrum can be achieved by multiplying both the real and imaginary Fourier amplitudes by a factor that varies as a function of the wavenumber. Hence, wave power is redistributed in the spectrum while wave phase is unchanged. The subtraction of a constant incremental power p representing the speckle-noise contribution from the total power P at all wavenumbers, while retaining the phase ϕ, can be accomplished with the following algorithms for the real, Re, and imaginary, Im, Fourier amplitudes:

$$Re = [(P-p)/(1+\tan^2\phi)]^{1/2} \quad \text{and} \tag{6}$$

$$Im = (P-p-Re^2)^{1/2} . \tag{7}$$

Since spectral power modifications are achieved without disturbing phase relations in the wavenumber domain, a Fourier inversion of the ocean-wave spectrum computed from a SIR-B intensity-variance spectrum yields an image of surface elevation that may be useful for monitoring wave groups that are inadequately characterized by their associated spectrum. Once a linear-modulation-transfer function for the SAR imaging of ocean waves is specified, image mean-and-variance statistics can be introduced in the Fourier restoration process and used to scale subsequent spectral-processing algorithms. The resultant wave-height estimates could be contoured directly in meters of surface elevation, but, since the absolute value of the modulations is still not well determined, such an absolute interpretation of the data may not yet be warranted. Nevertheless, the general procedure can be applied to all the SIR-B data for which we can assume a linear-modulation model. Moreover, with

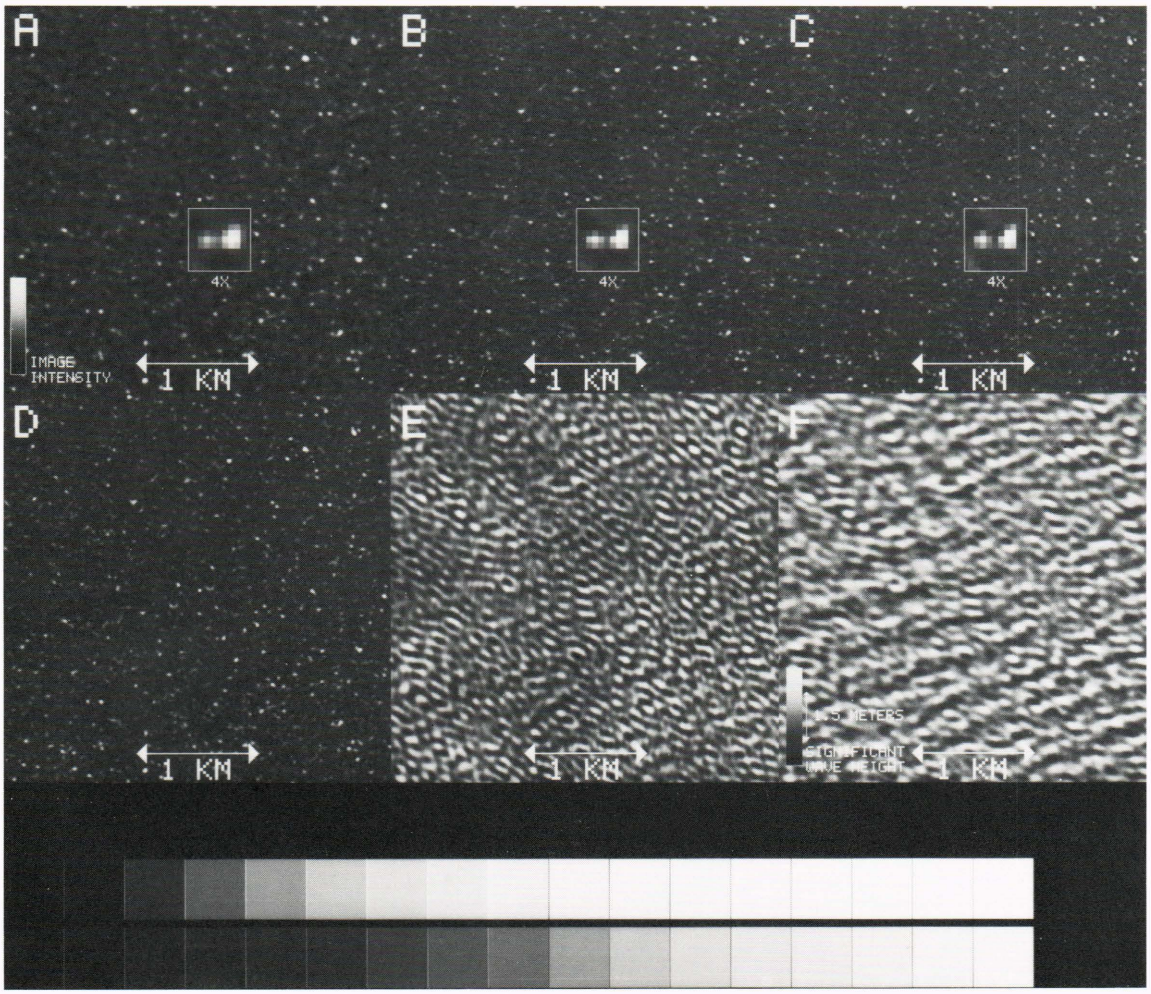

Figure 3—SIR-B imagery off the coast of Chile for a low sea state on October 10, 1984. Spatial resolution is somewhat improved in the image reconstructed after removal of the stationary response (B) as compared with the original SIR-B intensity image (A). Linear correction for the dynamic response function (C) visibly improves the resolution of doublets along track. Spectral smoothing for better wavenumber statistics appears to have little effect in the image (D) domain. Subtraction of an empirical noise pedestal in the Fourier domain reduces speckle noise in the image (E) domain. Lower spatial frequencies are emphasized when the wave-height perspective (F) is approximated with the best SAR hydrodynamic wave model that is currently available. Restored image wave height is represented by a vertical gray scale, with the $\pm 2\sigma$ deviation about the mean identified with an independent estimate of significant wave height.

an independent estimate of the spatially averaged significant wave height, each of the corrected SAR images can be annotated with an absolute wave-height gray scale.

SIR-B observed surface waves for a variety of environmental conditions, with significant wave height ranging from 1.5 to nearly 10 meters. During the last day of the SIR-B Extreme Waves Experiment (see also the articles by Monaldo and Beal, this issue) southwest of Chile, an ocean swell propagated along the SIR-B ground track with a wavelength of 360 meters and a significant wave height of approximately 3.5 meters. On the same day, SIR-B also observed 8- to 10-meter-high waves generated by Hurricane Josephine in the North Atlantic Ocean at a wavelength of 250 meters (see the article by Gonzalez et al., this issue) and a few days earlier observed a system of waves 2 to 3 meters high with a wavelength of 200 meters in the Agulhas Current off the southeastern coast of Africa (see the article by Irvine, this issue). These three data sets (Chile, Josephine, and the Agulhas) provide examples of both azimuth- and range-traveling waves, a large range of sea states, and a crossed sea complicated by a strong current. Figure 5 shows the resulting wave-height maps from each of three SIR-B data sets, after applying an identical five-stage adaptive filter in the Fourier domain to each of the corresponding radar-backscatter-amplitude maps. However, one should be cautious in accepting the height maps at face value. For example, isolated wave breaking with strong associated backscatter ("spikes") may well yield false indications of extreme events. On the other hand, isolated wave groups and the "lumpiness" properties characteristic of extreme seas (see the article by Mollo-Christensen, this issue) may very well be amenable to this type of analytic procedure.

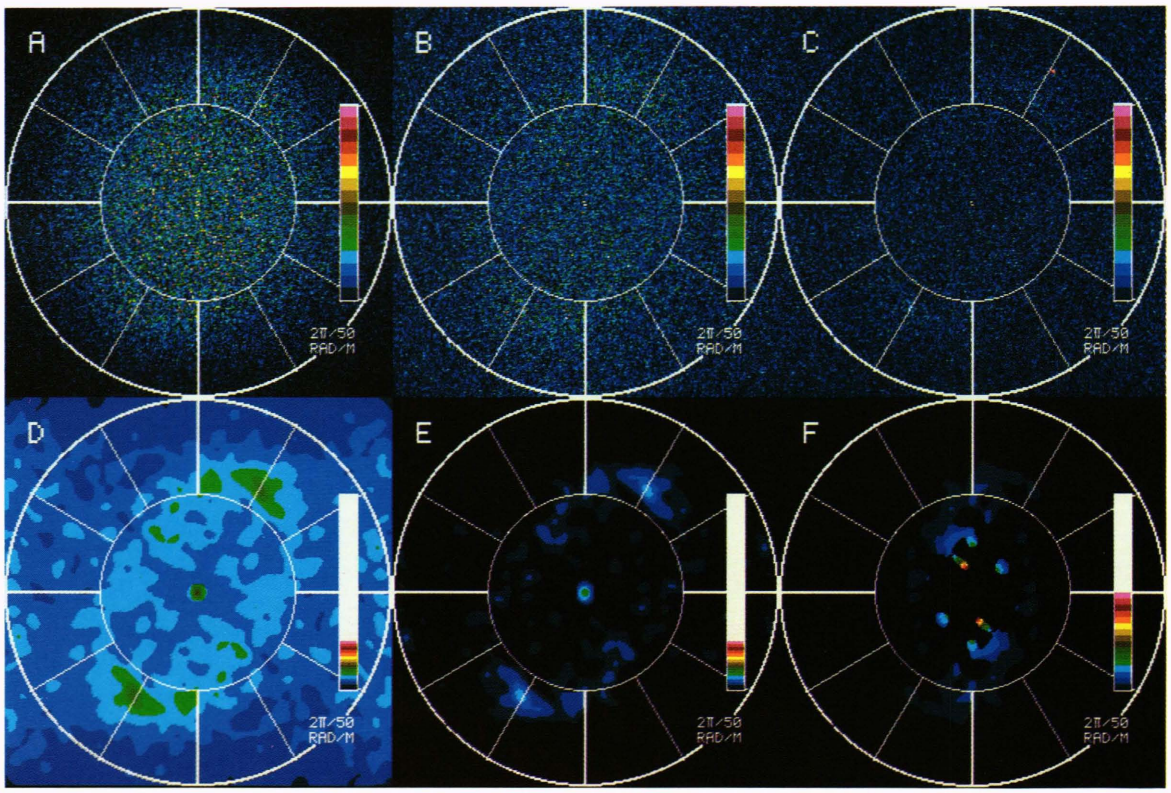

Figure 4—Uncorrected SIR-B spectra off the coast of Chile for October 10 (A). Removal of the stationary (B) and dynamic (C) transfer functions emphasizes higher wavenumber components and establishes a uniform noise floor. The spectrum after Gaussian smoothing (D) depicts a low power signal extending over a broad wavenumber domain. The subtraction of a broadband noise threshold (E) is complicated by specular sea clutter that is difficult to distinguish from low, steep wind-driven waves. The hydrodynamic modulation-transfer function suppresses the along-track spectral components at high wavenumber (F), which may not be appropriate for a specular signal. Note that the "true" wave spectrum on October 10 is highly distorted by the SAR (see Beal, Fig. 3, this issue).

CONCLUSIONS

Fourier restoration techniques applied to SIR-B ocean imagery in the Fourier transform domain can be used to estimate ocean-wave height. Linear filtering algorithms reduce the noise-to-signal ratio computed for SIR-B scenes of ocean waves. Each of the first three filtering operations reduces the spectral variance relative to the mean spectral density. The fourth operation reduces the mean but not the variance, and the final correction redistributes the spectral variance. Any asymmetry or skewing of the estimated wave-height distribution that increases with significant wave height could be taken as evidence of "groupiness" within storms. Clearly, however, much more work needs to be done in this area.

Instead of two independent range and azimuth polynomials, a two-dimensional polynomial is preferred for approximating the SIR-B stationary-wavenumber response function when the orthogonal ground coordinate resolutions are unequal. The accuracy of the estimate is improved at high wavenumbers by minimizing the squared fractional error. The linear correction for the dynamic wavenumber response of the SIR-B to surface motion partially restores azimuth resolution to the image and increases contrast at high wavenumber. A Gaussian convolution applied to smooth the ocean wavenumber spectra for more reliable measurements of wavelength and wave angle has little effect on spatial resolution when they are included as part of the Fourier filtering algorithm.

The modulation models for SAR observations of wind-generated waves are still not completely understood. The analysis of the low sea state off the coast of Chile on October 10 suggests that the tilt and modulation model should be extended to include a specular scattering component, due to high surface slopes, for wind-driven waves still in the process of forming a significant swell. In addition, the model employed here does not accommodate backscatter modulations that may be caused by nonuniform roughening of the ocean surface by a variable wind. Such scene-dependent modulations of the backscattered field will introduce additional complications in a SAR's perception of ocean waves that are not addressed in our present models and methods.

REFERENCES

[1] O. M. Phillips, "The Equilibrium Range in the Spectrum of Wind-Generated Waves," *J. Fluid Mech.* **9**, 193-217 (1958).
[2] R. C. Beal, D. G. Tilley, T. W. Gerling, D. E. Irvine, and F. M. Monaldo, "Spatial Variations of Ocean Wave Directional Spectra from the Seasat Synthetic Aperture Radar," *J. Geophys. Res.* **91**, 2433-2449 (1986).
[3] D. Witten, "Peril of the Rogue Waves," *NOAA Q.* **13**, 10-12 (1983).

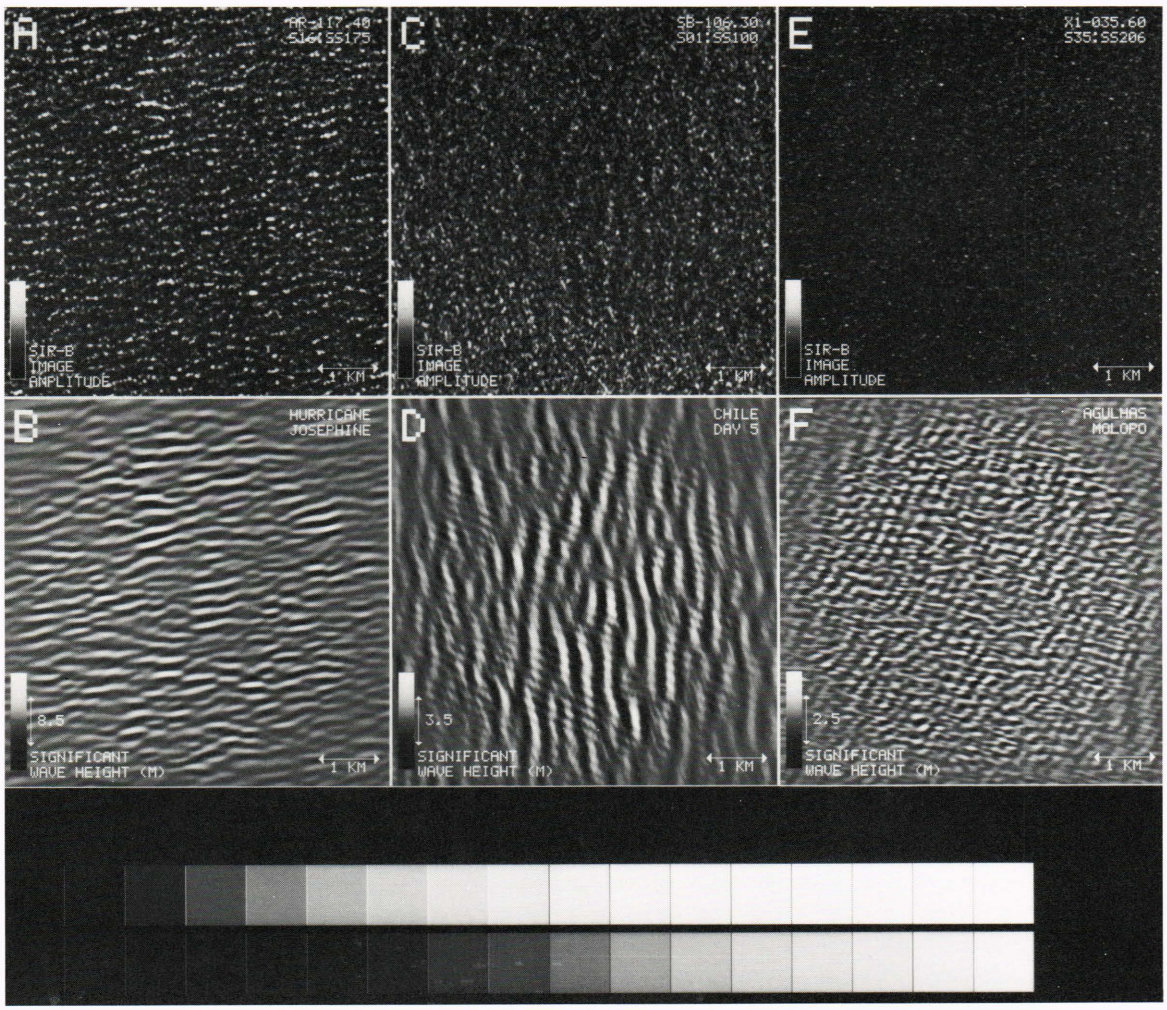

Figure 5—In frames (A) and (B), groups of range-traveling waves from the SIR-B Hurricane Josephine data set have been restored to the surface height perspective. In frames (C) and (D), a uniform field of azimuth-traveling waves from the Chile data set on October 12, 1984, has been processed with the same adaptive set of Fourier domain filters. In frames (E) and (F), a crossed sea state is interacting with the Agulhas Current off the coast of South Africa. Restored image wave height is represented by a vertical gray scale, with the $\pm 2\sigma$ deviation about the mean identified with an independent estimate of significant wave height.

[4]M. J. Tucker, "The Imaging of Waves by Satellite-Borne Synthetic Aperture Radar: The Effects of Sea Surface Motion," *Int. J. Remote Sensing* **6,** 1059-1074 (1985).

[5]W. Alpers, D. B. Ross, and C. L. Rufenach, "On the Detectability of Ocean Surface Waves by Real and Synthetic Aperture Radar," *J. Geophys. Res.* **86,** 6481-6498 (1981).

[6]W. Alpers, "Monte Carlo Simulations for Studying the Relationship Between Ocean Waves and Synthetic Aperture Radar Spectra," *J. Geophys. Res.* **88,** 1745-1759 (1983).

[7]N. E. Huang and S. R. Long, "An Experimental Study of the Surface Elevation Probability Distribution and Statistics of Wind-Generated Waves," *J. Fluid Mech.* **101,** 179-200 (1980).

[8]D. G. Tilley, "Use of Speckle for Estimating Response Characteristics of Doppler Imaging Radars," *Opt. Eng.* **25,** 773-780 (1986).

[9]D. G. Tilley, "Fourier Analysis of SAR Speckle for the Polynomial Synthesis of Spectral Corrections Applied to Seasat Oceanic Data," in *Digest, 1983 Int. Geoscience and Remote Sensing Symp.,* IEEE 83CH1837-4, Vol. II, FA-3, 4.1-4.6 (1983).

[10]J. S. Bendat, *Principles and Applications of Random Noise Theory,* John Wiley, New York, pp. 189-218 (1958).

[11]J. S. Bendat and A. G. Piersol, *Random Data: Analysis and Measurement Procedures,* John Wiley, New York, pp. 72-75 (1971).

[12]J. W. Wright, "A New Model for Sea Clutter," *IEEE Trans. Antennas Propag.* **AP-16,** 217-233 (1968).

[13]K. Hasselmann, R. K. Raney, W. J. Plant, W. Alpers, R. A. Shuchman, D. R. Lyzenga, C. L. Rufenach, and M. J. Tucker, "Theory of SAR Ocean Wave Imaging: The MARSEN View," *J. Geophys. Res.* **90,** 4659-4686 (1985).

[14]R. K. Raney, "Theory and Measure of Certain Image Norms in SAR," *IEEE Trans. Geosci. Remote Sensing* **GE-23,** 343-348 (1985).

[15]F. M. Monaldo and D. R. Lyzenga, "On the Estimation of Wave Slope- and Wave Height-Variance Spectra from SAR Imagery," *IEEE Trans. Geosci. Remote Sensing* **GE-24,** 543-551 (1986).

[16]A. D. Goldfinger, "Estimation of Spectra from Speckled Images," *IEEE Trans. Aerosp. Electron. Syst.* **AES 18,** 675-681 (1982).

[17]R. C. Beal, F. M. Monaldo, D. G. Tilley, D. E. Irvine, E. J. Walsh, F. C. Jackson, D. W. Hancock III, D. E. Hines, R. N. Swift, F. I. Gonzalez, D. R. Lyzenga, and L. F. Zambresky, "A Comparison of SIR-B Directional Ocean Wave Spectra with Aircraft Scanning Radar Spectra and Global Spectral Ocean Wave Model Predictions," *Science* **232,** 1531-1535 (1986).

ACKNOWLEDGMENTS—The internal consistency of the SIR-B data, processed at the Jet Propulsion Laboratory and provided by B. Holt in a format similar to the Seasat SAR data set, is appreciated. Oceanographic interpretations offered by R. C. Beal and D. E. Irvine of APL and by F. Gonzalez of the NOAA Pacific Marine Laboratory have been helpful, as were discussions of backscatter modulation with F. M. Monaldo of APL and D. R. Lyzenga of the Environmental Research Institute of Michigan. This work was funded by the NASA Office of Space Science and Applications.